Journal of Environmental Chemical Engineering 12 (2024) 114253

Contents lists available at ScienceDirect

Journal of Environmental Chemical Engineering

journal homepage: www.elsevier.com/locate/jece

Floating graphite felt-cellulose multilayer sandwich evaporator for solar salt-resistant seawater desalination: Mechanistic role of incorporated super water holding layer

Ridha Djellabi [a,b,*], Dominic Aboagye [a], Walid Nabgan [a], Francesc Medina [a], Sandra Contreras [a,**]

[a] Departament d'Enginyeria Química, Universitat Rovira i Virgili, Av. Països Catalans, 26, Tarragona 43007, Spain
[b] Department of Chemistry, Alfaisal University, Al Zahrawi Street, Al Maather, Al Takhassusi Road, Riyadh, 11533, Saudi Arabia

ARTICLE INFO

Keywords:
Solar-to-steam generation
Multilayer SSG structure
Seawater desalination
Salt rejection
Heat localization
Water holding cellulose

ABSTRACT

Solar-to-steam generation (SSG) for seawater desalination is emerging process which faces several technology challenges for successful scaling up. Floating solar-to-steam generation (SSG) sandwich-based systems using hydrophilic water bridges have been proved to be fascinating technology for seawater desalination. However, the mechanistic pathways of heat dissipation, mass diffusion and convection are still the key bottlenecks for reliable scaling up. To solve the heat loss and surface salt deactivation, we demonstrate herein the performance of novel SSG structure for seawater desalination via the incorporation of cellulosic sponge as water holder to play a role of water transit between hydrophilic bridge and the top surface. Two systems using low-cost materials were compared, namely graphite felt/hydrophilic paper/polystyrene (GF-HP-PS) and Graphite felt/Water receiver/hydrophilic paper/polystyrene (GF-HP-*WR*-PS). The process of heat generation and localization was maximum in the GF-*WR*-HP-PS system, reaching 68.2 °C under 0.5 sun. The photothermal conversion efficiency was found to be 92 and 114 % under 0.5 sun for GF-HP-PS and GF-HP-*WR*-PS, respectively. On top of that, GF-HP-*WR*-PS shows effective steadily salt rejection during the desalination of seawater. The *WR* layer plays a crucial role to govern the confined water, which boosts the dissolution of salt and its convection without significant heat downward convection. As a practical consideration, the cost of used components to fabricate this SSG system is very acceptable and without major restrictions.

1. Introduction

As a result of the extensive worldwide population along with huge agro-industrial activities, many issues have been raised over the last decades that threat the current and future generations. Environmental pollution and high energy deemed are at the top of the list, pushing the scientific and industrial worldwide organizations to seek for urgent solutions [1]. In fact, these issues are directly associated with the linear economy approach that have been applied since the industrial revolution to fulfill the economic needs, and up to date this approach is still in action in many countries and regions [2]. Water is the most important natural resource in our planet for humankind's survival. Freshwater is essential for all agro-industrial processes and human daily use [3]. Nowadays, many countries are suffering from water scarcity and water pollution which require the design of processes to clean and desalinate water [4]. The World Bank group reported that about 1.6 billion people living in remote areas will not have access to clean water by 2030, which put their lives in danger. Over the last decades, the circular economy approach has come into action to solve environmental, energy and socio-economic challenges, which belong to the sustainable development and zero carbon emissions [5,6]. Circular economy (CE) is a general concept having different definitions in the literature [7]. Shortly, it is based on the use of sustainable and clean processes in different fields. The management of agro-industrial wastes, by their recycling or/and valorization into valuable products, is a core in CE [8,9]. Certainly, the use of solar light to drive environmental or energy production processes is considered as green path to limit the over consumption of natural resource such as fossil fuels [10,11]. Solar driven

* Corresponding author at: Departament d'Enginyeria Química, Universitat Rovira i Virgili, Av. Països Catalans, 26, Tarragona 43007, Spain.
** Corresponding author.
E-mail addresses: rdjellabi@edu.edu (R. Djellabi), sandra.contreras@urv.cat (S. Contreras).

https://doi.org/10.1016/j.jece.2024.114253
Received 17 July 2024; Received in revised form 5 September 2024; Accepted 24 September 2024
Available online 25 September 2024

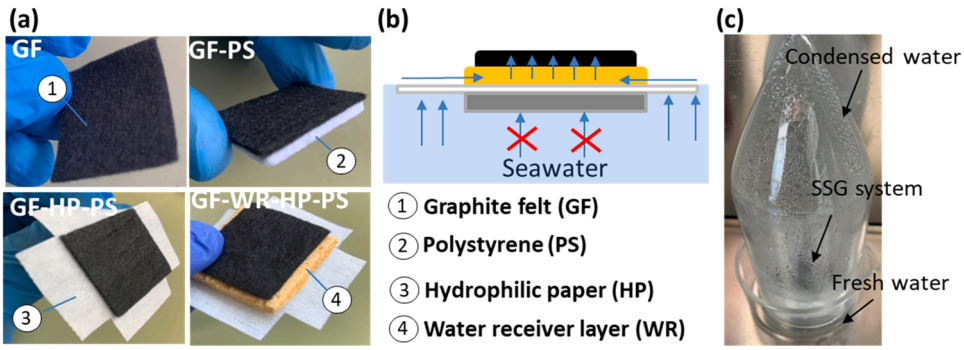

Fig. 1. (a) Components to build photothermal material. (b) Scheme showing GF-HP-W*R*-PS. (c) Image of the photothermal reactor showing the condensation of steam.

photothermal process, so-called solar-to-steam generation (SSG), has received a lot of attention to be used for seawater desalination [12]. On top to seawater desalination, SGG application has been widened to further emerging processes including in energy production [12], wastewater treatment [13], electricity generation [14] and so on. Freshwater production via photothermal process is very similar to the natural hydrological cycle [15]. It is based on the heating of top surface, excluding bottom water, to boost the conversion of water into steam, to be condensed as fresh water. Even though SSG processing is very simple and low-cost, many technological issues have been raised limiting the real world application [16]. Materials with high light absorption and light to heat production abilities should be designed to be used as photothermal layer (top surface). A desired photoabsorber would have broad solar light harvesting from 300 to 2500 nm, along with reduced light reflection [17]. Several materials can be used as photoabsorber such as carbon materials [18], polymers [19], metal oxides [20], semiconductors [13] and plasmonic nanoparticles [21]. The localization of produced heat is the most crucial step to maximize the water into heat generation. The heat can be lost through two different processes, namely heat convection and heat emission in the air. The heat convection is a natural mechanism wherein the heat moves from the hottest area to coldest. Therefore, thermal-insulator bilayer structure is required to avoid the transfer of heat from the top to the bulk water. The nature of insulator is very crucial which should exhibit three main features such as excellent thermal-insulation, good wettability to pomp the water from the bulk to the top surface and good salt rejection ability [22]. In general, having all these factors in one single material is very difficult, and therefore, a tradeoff among them is usually accepted [23–25]. To bridge between salt rejection and heat localization, Zhang *et Li.* designed a photothermal system with a fluidic flow in a wick-free confined water layer, wherein macrochannels were created to reject the salt through the natural convection process [26]. Three layers sandwich configuration wherein the hydrophilic layer is placed between the photothermal absorber and the non-porous insulator has been proved to be excellent for heat localization as compared to traditional double layer based SSG systems [16,27]. The so-called tree configuration is one of the latest suggested SSG systems wherein the photothermal surface is located in the air far from the water surface and bridged with water using hydrophilic column to transport water from the bottom to the top photothermal surface [28]. In this case, the localization of heat can be maximized, while the salt rejection from the surface becomes more challenging [29]. The stability of the materials that can be used for long-term in seawater under solar irradiation is very important factor. Most of photothermal materials are obtained via chemical processes by coating of nanoparticles or/and designing aerogels and polymers as photothermal or insulators which might result in weak stability especially in harsh seawater conditions.

Herein, we report a new SSG configuration using commercially low-cost available materials. A new layer so-called water reservoir was inserted between the insulator and the top photoabsorber surface as water transit layer, which in turn limits the heat convection and allows excellent salt rejection at the same time. In conventional multilayer SSG systems, the hydrophilic layer connects directly the photothermal surface and bottom water which results in huge heat loss due to the convection. The mechanisms of heat localization, steam generation and salt rejection for seawater desalination were discussed on the novel SSG configuration compared with conventional SSG sandwich process. The role of water holder layer to govern the confined water was investigated was for the first time in this study, and the mechanisms to insulate the heat and facilitate the convection of salt were studied.

2. Materials and experimental

Herein, new SSG configuration was structured with an aim to solve the issue of heat loss, meanwhile the salt rejection can be achieved effectively. Materials used in this SSG configuration are commercially available and chemically stable. The cost-effective SSG system can be designed without the need of any chemical to avoid all contamination during the evaporation process. The combination of different parts of the SSG system was achieved using a thread and needle. The designed photothermal system is shown in Fig. 1**a**. Graphite felt (GF), purchased from Shanghai Hesen Electrical Co., Ltd, was used as solar photothermal absorber (7.4 cm^2). Polystyrene (PS) sheet was used as floating material to support GF photoabsorber. The system graphite felt fixed on polystyrene is abbreviated as GF-PS. The introduction of hydrophilic paper (HP) between graphite felts fixed on polystyrene forms three-layer GF-HP-PS sandwich. The addition of water receiver layer (W*R*) between GF and HF (yellow layer) forms GF-HP-W*R*-PS sandwich system. HP and W*R* are made of cellulose, and they were obtained from local shops. The scheme of GF-HF-W*R*-PS is shown in Fig. 1**b**. Lab photothermal experiments were carried out in Suntest CPS+ATLAS solar simulator with maximum intensity of 500 W/m^2 (0.5 sun). Glass photothermal reactor is composed of three parts: beaker containing seawater and floatable photothermal material, water condenser which covers the beaker to condense the steam into freshwater and freshwater receiver (Fig. 1**c**). Seawater samples were collected periodically from the Mediterranean Sea in the region of Tarragona, Spain. 200 mL of seawater is placed in the beaker and then the material is placed on top water, then the beaker is covered and placed inside the solar simulator. During the photothermal experiments, the weight of the water is followed continuously by a balance to estimate the quantity of evaporated water. The heat generation over the experiments is followed using an Nf-521 infrared thermal imager camera. The concentration of cations before and after desalination was measured by 7800 ICP-MS Agilent instrument. SEM-EDS was performed on a scanning electron microscope operating with a Field Emission source (FE-SEM LEO 1525 ZEISS equipped with a Bruker Quantax EDX). XRD analysis of GF, HP and W*R* samples was carried out on X-ray diffraction (XRD) equipment with a Cu Kα radiation

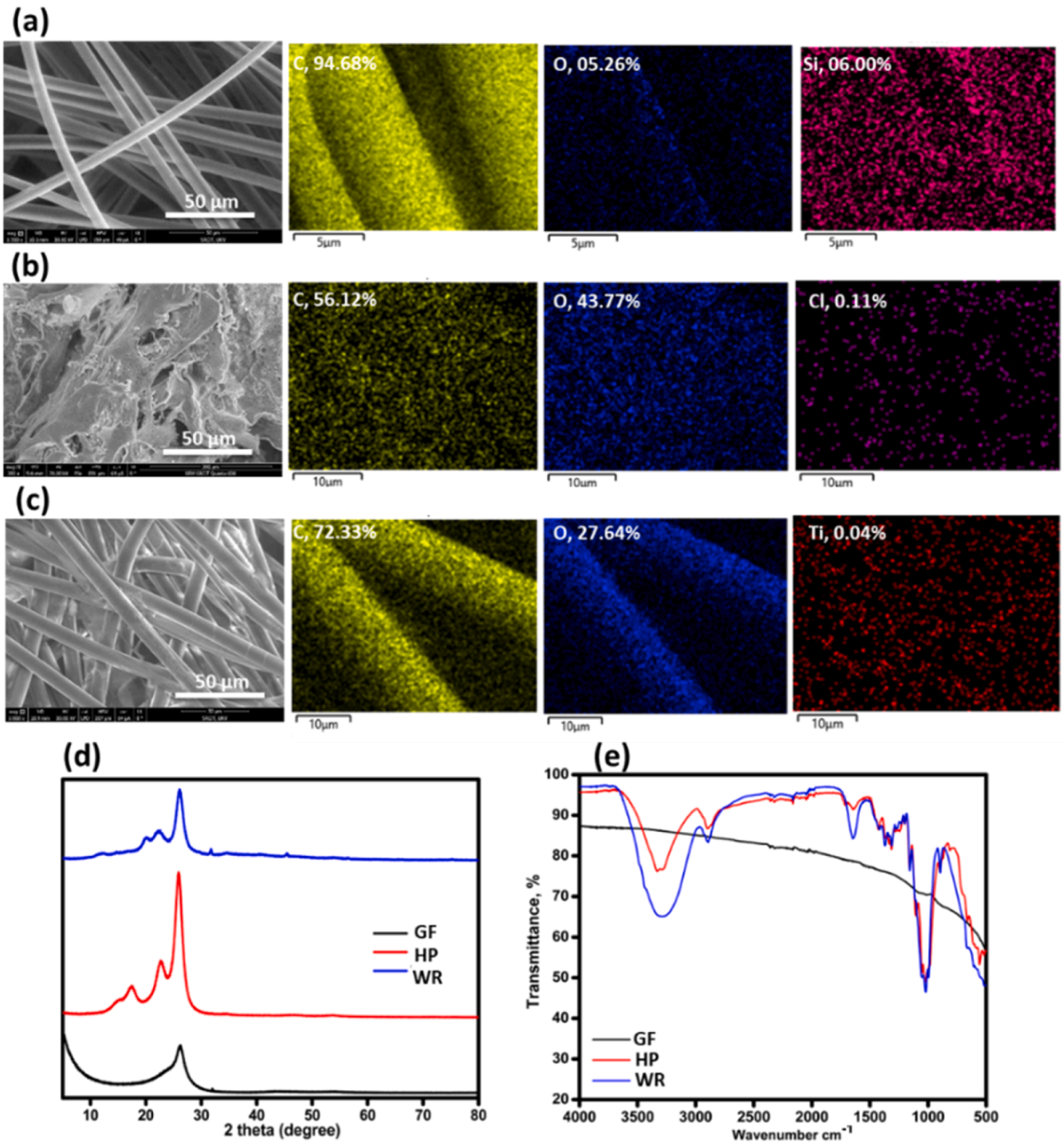

Fig. 2. (a) SEM image and EDX mapping of graphite felt (GF), (b) SEM image and EDX mapping of cellulosic water receiver layer (*WR*), (c) SEM image and EDX mapping of hydrophilic paper (HP). (d) XRD patterns of GF, *WR* and HP; e) FTIR spectra of GF, *WR* and HP.

(wavelength $\lambda = 1.5418$ Å), operating at 40 kV and 30 mA. FT-IR spectra were recorded on Jasco FT/IR-600 Plus instrument equipped with a Specac Golden Gate™ attenuated total reflectance (ATR) device.

3. Results and discussion

Fig. 2 shows SEM-EDX, XRD and FTIR analysis of graphite felt (GF), cellulosic water receiver layer (*WR*) and hydrophilic paper (HP). SEM and EDX mapping images of GF are shown in Fig. 2**a**. SEM image shows cross-linked carbon fibers of about 5–7 µm. Carbon fibers form multilayer solid structure with high porosity which could improve the absorption of light, and reduce its refection into the air [30]. In addition, this structure would be excellent to store the produced heat and to reduce the heat emission. Highly porous materials as top surface in SSG are also recommended because of their ability to reject the salt as compared to less or non-porous surface [16,31]. EDX mapping images show that GF is made mostly of carbon along with oxygen and trace of silicon. In other images (not shown here), trace of nanoparticles of Fe incorporated in the carbon fibers was also noticed. SEM and EDX mapping images of *WR* are shown in Fig. 2**b**. This material was obtained

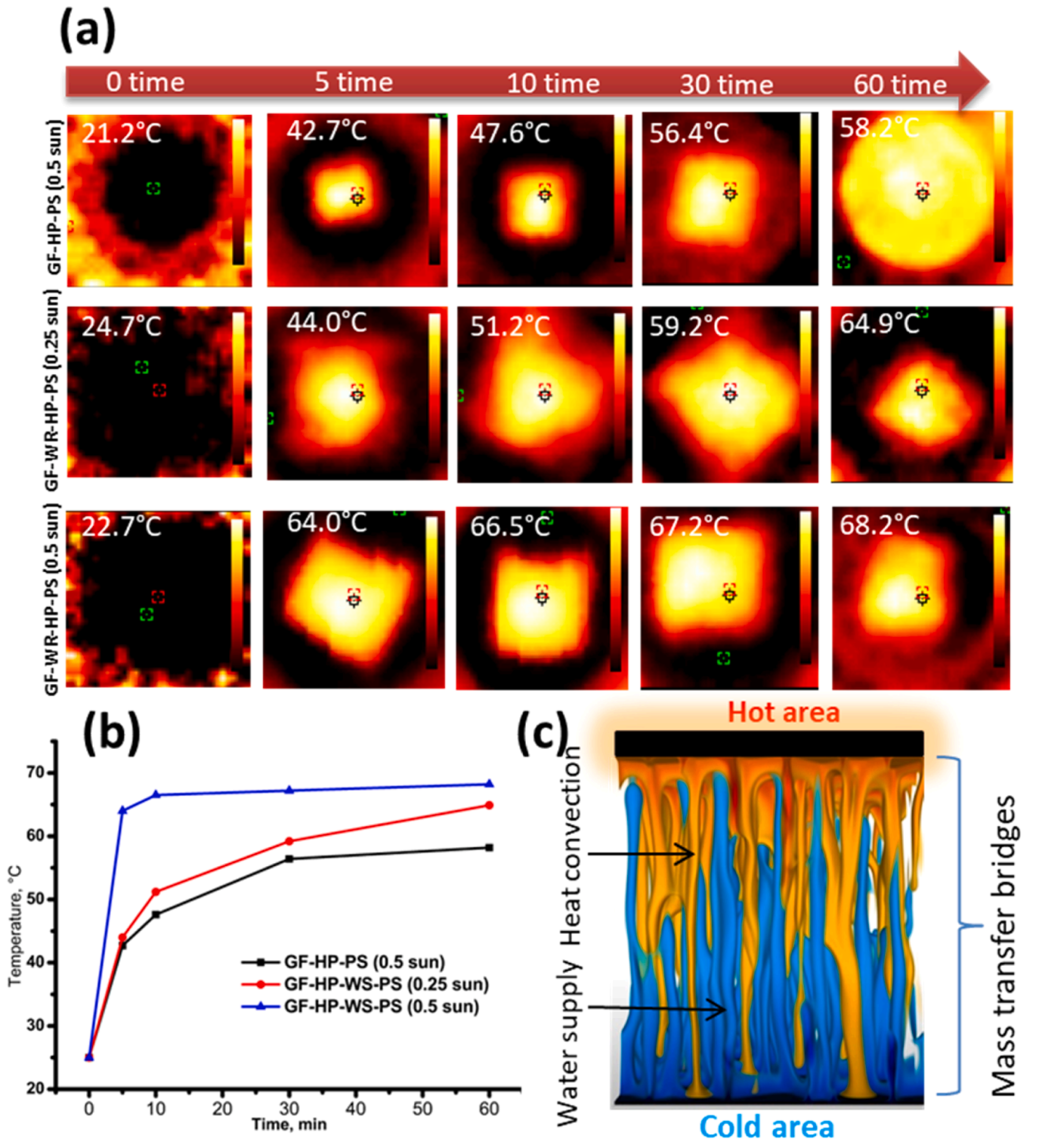

Fig. 3. (a) Photothermal images during seawater desalination on different systems. (b) Curves showing the increase in temperature on the top surface of GF-HP-PS and GF-W*R*-HP-PS systems. (c) Scheme explains the heat loss through mass transfer bridge (insulator) in SSG process.

from a local shop, and it is made of natural cellulose. It can be seen that W*R* consists of carbon and oxygen. Natural cellulose sponge can hold water up to 20 times than its wet state due to its high hydrophilicity and compressing properties. Fig. 2**c** shows SEM and EDS mapping images of HP. SEM image shows crossed linked carbon fibers with high density. The high content of oxygen in HP and W*R* compared to GF reflects their cellulosic nature. In general, the high incorporated oxygen content in a given material results in better wettability [32]. In fact, the presence of high yield of oxygen leads to more hydrogen bonding and high polarity, which in turn allow the absorption of water molecules [33]. Based on EDX images, W*R* sample exhibits higher oxygen content that HP. For that reason, W*R* shows outstanding water absorption and condensation to supply the top surface to generate steam and dissolve salt, as it will be discussed in the next sections. XRD patterns of GF, W*R* and HP are shown in Fig. 2**d**. GF shows a strong diffraction peak positioned at around 26.4° due to (002) plane of graphite crystallite, while a weaker peak at 44°

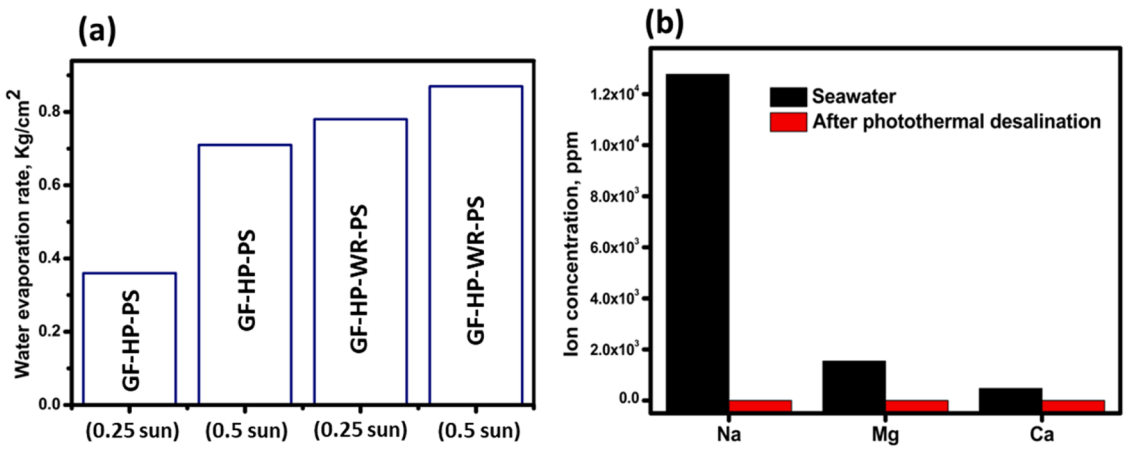

Fig. 4. **(a)** Evaporation rates of GF-HP-PS and GF-HP-W*R*-PS systems. **(b)** Concentration of Na(I), Mg(II) and Ca(II) cations before and after solar desalination using GF-HP-W*R*-PS.

related to (010) crystal plane [34]. W*R* curve shows three main diffraction peaks at 20°, 22.5° and 26°, while HP shows diffraction peaks at 17.5°, 22.5° and 26°. These three peaks are corresponded to planes of (110), (110) and (200), respectively [35]. Fig. 2**e** shows FTIR spectra of GF, W*R* and HP. GF does not show peaks which proves the chemical inertness of bulk graphite [36]. HP and W*R* spectra show similar bands that are related to cellulose vibrations [37,38]. Main peak at 1100 cm^{-1} is due to C-O stretching vibrations. Peaks located at 1620 cm^{-1} are due to adsorbed water molecules. The wide band at around 3400 cm^{-1} corresponds to hydroxyl groups. It can be seen that both bands related to water molecules and hydroxyl groups are more intense in the case of W*R* sample as compared to HP sample, which confirms the higher oxygen content and wettability. The use of cellulose based materials to design this system is due to their excellent characteristics for good mechanical force, heat insulation, water transport and low cost [38,39]. Due to their hydrophilicity [40,41], cellulosic fibers are amenable to construct water bridges thanks to their channel based structure. On top of that, cellulose materials have excellent heat insulator, which helps to localize the photothermal produced heat. The thermal conductivity and the thermal diffusivity of cellulose are 0.039 W/mK and 0.046 $\times 10^{-6}$ m^2 /s, respectively [42,43].

SSG process for seawater desalination depends on several factors. The first factor that needs to be studied is the heat production and localization. The localized heat is the main responsible for occurring steam production. Graphite felt, known as an carbon based electrode [44,45], was used as the photoabsorber material due to its high solar light absorption and light-to-heat conversion. On top of that, due to the macro-porosity, the heat emission into the air can be reduced and saved within the porous. Photothermal materials with highly porosity allow intense microscopic light reflection inside the porous, which in turn may multiple the absorption of light and improve the yield of produced heat. Many reports mentioned that porous materials are more effective for light absorption and heat localization as compared to flat materials [46, 47]. IR images of GF-HP-PS and GF-HP-W*R*-PS during photothermal seawater desalination were taken at different time intervals and the results are shown in Fig. 3**a,b**. Similar to graphene, graphite material exhibits zero band gap, which reflects its high electricity and heat conductivity due to the freely movement of electrons through it [48,49]. The zero-band gap allows the wide light absorption capacity. Due to its relatively good specific heat, GF could manage the produced heat within itself, preventing high emission. A material with high heat capacity is likely good to store heat for a given time to be used for the evaporation process, and the reverse is true. Using the graphite filter alone (GF), the localization of heat on the surface is not possible (data not shown). The produced heat is immediately released in bottom water. The complete release of heat from top surface to bottom water does not lead to steam production especially in large water volumes as the heat will be diluted closer to bulk water temperature. The use of GF supported on polystyrene sheet (GF-PS) shows a relative localization of heat within the first 10 min, but afterword the heat starts to be released into bulk water similar to the case of GF (data not shown). In addition, in GF-PS system, there is no way to supply water from the bottom to the top surface, which suppresses the evaporation step. In the scenario where hydrophilic paper is placed between the GF and PS to obtain GF-HP-PS sandwich, better heat localization was found. Within 5 min, the produced heat on the top surface reaches 42.7°C, and 58.2 °C after 1 h. However, there is a relative release of heat to bulk water starting from 30 min. The role of HP is to pump the water from the bottom to the top surface because of its highly hydrophilic ability. On top of that, HP layer plays an important role as insulator to boost the localization of heat. Photothermal images taken on GF-HP-W*R*-PS system at 0.25 and 0.5 sun prove the super localization of heat over time. Under 0.25 sun, the heat production efficiency and speed were better as compared to GF-HF-PS under 0.5 sun. The produced heat reaches 44 and 64.9°C within 5 and 60 min, respectively under 0.25 sun. Under 0.5 sun, the production of heat was very intense within just 5 min, which reaches 64°C, raising to 68.2 °C after 1 h. The layer of W*R* is very important to maximize the heat insulation. The management of produced heat is extremely important for effective photothermal steam production process [50]. In ideal scenario, the produced heat is used entirely for the heating of surface water into steam. However, partial heat loss is inevitable in real systems via two main process including heat downward convection to bottom water (Fig. 3**,c**), and upward heat emission into the air. In fact, heat downward convection in bulk water is the fastest way due to the high thermal-conductivity of water of 0.598 $Wm^{-1}K^{-1}$ at 20°C [51]. Besides, the heat convection is boosted with mass transfer. In other terms, the movement of salt by diffusion or convection from the top surface to the bulk water pushes the movement of considerable heat as well. The engineering of ideal SSG system should balance between an excellent salt convection and delayed or slow heat convection. Most of reported studies have investigated the design of thermal-insulator-supported bilayer/trilayer based SSG to limit the downward heat dissipation [52, 53]. However, in these conventional SSG systems, hydrophilic bridges connect directly the top surface with the bulk water (direct water pumping and direct salt convection). In GF-HP-W*R*-PS system, W*R* layer plays a crucial role to limit the direct interaction of supplied cold seawater and the produced heat wave. It collects first the water pupped by HP wingers, and then it passes to top surface. The connection of heat is restricted because W*R* plays the role of insulator to reduce the contact of heat with HP bridges, wherein a higher speed of cold-water circulation takes places.

The designed photothermal materials were tested to desalinate real

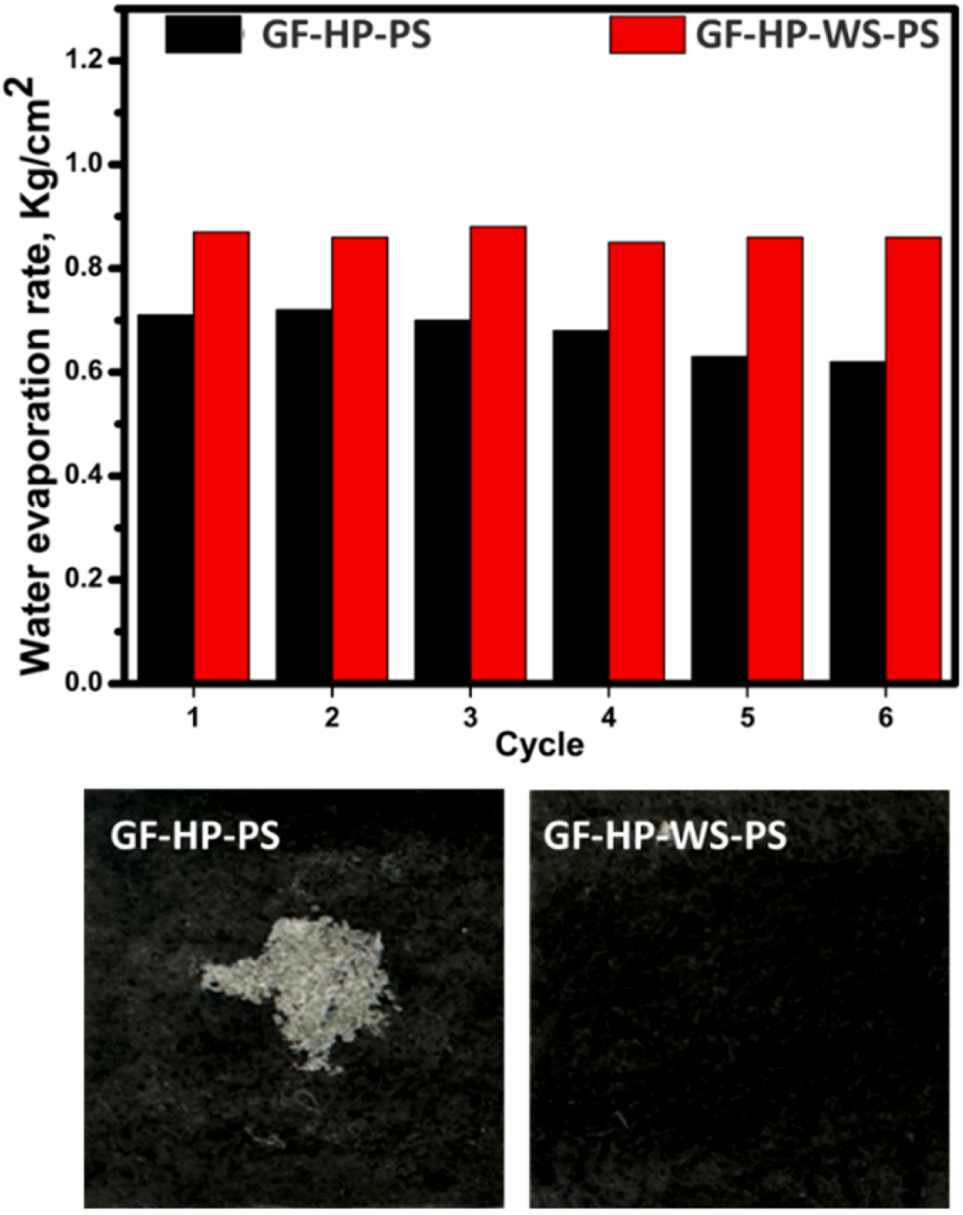

Fig. 5. Recycling of GF-HP-PS and GF-HP-W*R*-PS for seawater desalination under 0.5 sun. Insert images, left: image of GF top surface of GF- HP-PS, right: image of GF top surface of GF- HP-W*R*-PS.

seawater (Mediterranean Sea, Tarragona, Spain). The results of seawater desalination using GF-HP-PS and GF-HP-W*R*-PS systems in terms of evaporation rate are shown in Fig. 4**a**. Overall, it can be deduced that the better the heat is localized, the better the water evaporation rate is obtained. To estimate the performance of photothermal processes to produce fresh water from seawater, several parameters must be considered. In general, the specific water productivity (SWP) should be used to show the amount of fresh water per irradiated surface of the photothermal system [16,54,55]. Interestingly, GF-HP-W*R*-PS showed excellent photothermal activity even under low intensity (0.25 sun), suggesting its high performance to accumulate the light irradiation and convert it into heat. As before discussed, the high porosity and crossed lines structure of GF allow multiplying light reflections, which in turn boosts the heat production. From the large-scale point of view, the steam production at low solar intensity is highly recommended as it allows the application of technology in less sunny conditions. On top of that, it can be mentioned that W*R* layer plays an important key to localize the heat. At 0.25 sun, GF-HP-W*R*-PS shows better evaporation rate compared to GF-HF-PS at 0.5 sun. The photothermal conversion efficiency was found to be 92.32 and 113.85 % under 0.5 sun for GF-HP-PS and GF-HP-W*R*-PS, respectively, which confirms the significant improvement in solar-to-heat conversion performance due to the novel design. After the desalination of seawater GF-HP-W*R*-PS, the concentration of Na(I), Mg(II) and Ca(II) were dramatically decreased to 54.53, 45.92 and 13.88 ppm, respectively (Fig. 3**b**). It is important to mention that these concentrations are lower than the recommended norms by WHO in drinking water, which are fixed at 200, 150 and 75 ppm for Na(I), Mg(II) and Ca (II), respectively [56].

In SSGs, the continuity of the process is a very important factor to facilitate the scaling up. The photothermal system can be degraded due to the harsh seawater conditions, biofouling and salt accumulation. One of the purposes of this investigation is to solve the surface deactivation by accumulated salt. In general, the transport of salt from the top surface to the bottom medium is carried out through two mechanisms, namely mass flow diffusion ($J_{diffusion}$) and mass flow convection ($J_{convection}$) via microchannels in the photoabsorber and insulator pushed by the os-

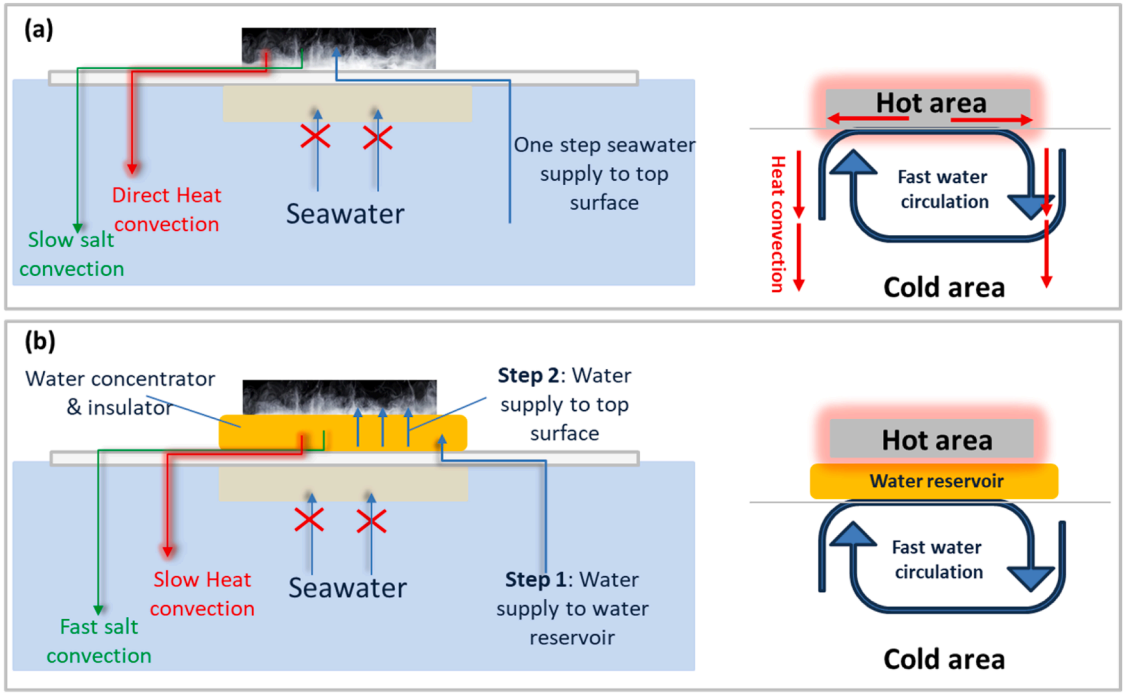

Fig. 6. Functionality of **(a):** GF- HP-PS and **(b):** GF-HP-W*R*- PS photothermal system for seawater desalination.

motic driving force and gravity [55,57]. The rate of salt mass (*J*) transfer from the top surface to the bottom water is represented by Eq. 1.

$$J = J_{diffusion} + J_{convection} = nA\varepsilon\left(\frac{k_d(C_{evp} - C_0)}{l} + k_c(\rho_{evp} - \rho_0)\right) \quad (1)$$

Where, n is the number of aligned mass transfer bridges (MTBs) exhibiting vertically hydrophilic microchannels to connect the top surface region with bottom seawater. MTBs are the key factor for the salt rejection in SSG systems. Therefore, the design of insulator with high number of MTBs is highly required to boost the transfer of salt through the convection and diffusion processes. MTBs are characterized by cross-section area (A), porosity (Ɛ), and height (*l*). k_d and k_c are the salt average diffusion and convection coefficients, respectively. C_{evp} and C_0 represent the concentration of salt on top surface and bottom seawater, respectively. ρ_{evp} and ρ_0 the densities of salt solution on top surface of evaporator and bottom seawater, respectively.

In fact, the salt convection boosts automatically heat convection which reduces the localization and water evaporation. In other words, the convection of heat is more pronounced in saline water as compared to less or non-saline water. The main bottleneck to design a reliable photothermal system is the compromise between super salt rejection and maximum heat localization [58]. This matter remains elusive up to date as the salt transport during solar evaporation is a complicated process [25,55]. In typical scenario, water is supplied from the bulk water to the top surface through MTBs to ensure the evaporation, and then part of this water should come back to bottom water, carrying with it the salt by convection in circulation mode. The total evaporation of pumped water leads to dry immediately the surface and salt crystals will appear within a certain time. These crystallization cycles end by the formation of salt layer on the surface of evaporator. As reported by Eq. 1, the number of aligned mass transfer bridges (MTBs) can govern the supply of seawater from bottom to the top surface and the salt convection by adjusting the number of vertical hydrophilic microchannels. However, as mentioned above, the salt convection and heat convection occur simultaneously. Therefore, the introduction of high number of vertical hydrophilic microchannels to reject the salt might simultaneously lead to significant heat loss by convection. A trade-off between these factors is usually obtained for a continuous process. For this purpose, the amount of confined water, which is defined as the water in touch with the photothermal area, should be optimized to get a tradeoff between heat localization and boosts mass diffusion. To estimate the role of confined water towards the salt rejection governed by W*R* layer, recycling tests of GF-HF-PS and GF-HF-W*R*-PS systems were carried for six times in row without cleaning the surface between each experiment and the results are shown in Fig. 5. In terms of GF-HP-PS, the efficiency decreases slightly along with the appearance of salt crystals especially in the middle of the evaporator. It can be deduced that there is less confined water in the middle of evaporator to dissolve the salt continuously and properly. It is believed that the heat production and localization would be maximized in the middle of the evaporator, which leads to fast evaporation and a dried surface. In the case of GF-HF-W*R*-PS, neither decrease in the efficient nor salt formation was observed. W*R* layer keeps the bottom of the GF surface wet, which in turn boosts the immediate dissolution of salt, keeping the surface clean and active.

The plausible mechanisms of photothermal seawater desalination on GF-HP-PS and GF-HP-W*R*-PS systems were schematized in Fig. 6. Starting by water supply, in the case of GF-HP-PS, the water moves from bottom bulk seawater directly to surface through HP wingers. The non-porous PS floating support does not allow the passage of seawater from the bottom. The supply of water through hydrophilic wingers is a great option to avoid the dissipation of heat. Based on the results of photothermal heat production, HP wingers can contribute to the loss of heat, which is inevitable. HP bridges directly cold area and hot area which certainly pushes the heat convection, and in addition, the cold supplied water could cool down the hot confined water. The accumulation of salt on the surface of GF-HP-PS evaporator was not observed quickly; however, after several recycling runs, the salt appears clearly. The convection of salt in GF-HP-PS is a slow process, which is due to the low confined water, allowing the drying of surface and salt formation. In GF-HP-W*R*-PS system, the supply of seawater passes through two steps: the first one relies on the movement of water through HP from bulk water to hydrophilic water reservoir (W*R*) which will be accumulated as confined water, and the second step is the movement of water from W*R* layer to top surface. This design limits the direct contact of hot area (top surface) with bulk cold seawater through HP bridge, which in turn prevents the

release of heat as discussed in the case of GF-HF-PS. Cellulose W*R* layer meanwhile serves as a heat insulator, reinforcing the localization of heat on the top surface. Regarding the salt rejection, the mechanism is carried out by continuous dissolving of salt and its fast convection due to the high yield of confined water collected in W*R* layer. Because of the high water holding capacity of cellulose W*R* layer, the top surface of GF photothermal absorber never reaches a dried state. As soon the water on the top surface is evaporated, a new water wave reaches the surface, keeping a continuous wettability of the top surface and good water circulation between the GF top surface and W*R* layer. In such an environment, the salt can be rejected from the top surface through two mechanisms, involving the flow diffusion and mass flow convection. The vertical displacement of salt driving by gravity is more pronounced in pores and wet surface. The confined water carries the salt through pores and channels of W*R* layer and HP. On top of that, salt convection caused by natural osmotic process is a very dominant phenomenon.

4. Conclusions

This study reports the design of a new SSG configuration to overcome two of the main issues of this technology, including the heat loss and surface salt deactivation. We demonstrate that the incorporation of new water holding layer between the photothermal top surface and hydrophilic bridges limits the convection of salt and boosts the diffusion and convection of salt. The comparison between the conventional GF-HP-PS sandwich configuration and novel GF-HP-W*R*-PS configuration has led to prove that the incorporation of water holding layer was behind the insulation of produced heat and the dissolution of salt in continuous way. In terms of conventional GF-HP-PS, the localization of heat was not a steady process, wherein clear heat dissipation was observed within 1 h. The photothermal conversion efficiency was found to be 92 and 114 % under 0.5 sun for GF-HP-PS and GF-HP-W*R*-PS, respectively. The performance of heat production and seawater desalination was much better using GF-HP-W*R*-PS at lower solar intensity (0.25 sun). Overall, the novel suggested configuration using low-cost cellulosic and carbon materials could help to design SSG systems for continuous and effective seawater desalination.

Declaration of Competing Interest

The authors declare that they have no known competing financial interests or personal relationships that could have appeared to influence the work reported in this paper

Data Availability

No data was used for the research described in the article.

Acknowledgements

This work was supported by Grant PID2021–123665OB-I00 funded by MCIN/AEI/10.13039/501100011033/ and by “ERDF A way of making Europe”. Dr Ridha Djellabi acknowledges Maria Zambrano Grants-2021URV-MZ-15.

References

[1] M.Z. Jacobson, Review of solutions to global warming, air pollution, and energy security, Energy Environ. Sci. 2 (2009) 148–173.
[2] M. Sillanpaa, C. Ncibi, The circular economy: case studies about the transition from the linear economy, Academic Press, 2019.
[3] J. Schornagel, F. Niele, E. Worrell, M. Böggemann, Water accounting for (agro) industrial operations and its application to energy pathways, Resour., Conserv. Recycl. 61 (2012) 1–15.
[4] R. Arikrishnan, N. Rajendran, Research trends in water scarcity: a world perspective, Libr. Philos. Pract. (2021) 1–9.
[5] H. Corvellec, A.F. Stowell, N. Johansson, Critiques of the circular economy, J. Ind. Ecol. 26 (2022) 421–432.
[6] T.G. Ambaye, R. Djellabi, M. Vaccari, S. Prasad, T. Aminabhavi, S. Rtimi, Emerging technologies and sustainable strategies for municipal solid waste valorization: challenges of circular economy implementation, J. Clean. Prod. (2023) 138708.
[7] S. Geisendorf, F. Pietrulla, The circular economy and circular economic concepts—a literature analysis and redefinition, Thunderbird Int. Bus. Rev. 60 (2018) 771–782.
[8] Y. Geng, J. Sarkis, R. Bleischwitz, How to globalize the circular economy, Nature 565 (2019) 153–155.
[9] R. Djellabi, P. Su, E.A. Elimian, V. Poliukhova, S. Nouacer, I.A. Abdelhafeez, N. Abderrahim, D. Aboagye, V.V. Andhalkar, W. Nabgan, Advances in photocatalytic reduction of hexavalent chromium: from fundamental concepts to materials design and technology challenges, J. Water Process Eng. 50 (2022) 103301.
[10] D. Aboagye, R. Djellabi, F. Medina, S. Contreras, Radical-mediated photocatalysis for lignocellulosic biomass conversion into value-added chemicals and hydrogen: facts, opportunities and challenges, Angew. Chem. Int. Ed. 202301909 (2023) 29.
[11] M. Mergbi, M.G. Galloni, D. Aboagye, E. Elimian, P. Su, B.M. Ikram, W. Nabgan, J. Bedia, H.B. Amor, S. Contreras, Valorization of lignocellulosic biomass into sustainable materials for adsorption and photocatalytic applications in water and air remediation, Environ. Sci. Pollut. Res. (2023) 1–31.
[12] C. Chen, M. Wang, X. Chen, X. Chen, Q. Fu, H. Deng, Recent progress in solar photothermal steam technology for water purification and energy utilization, Chem. Eng. J. 448 (2022) 137603.
[13] I. Ibrahim, D.H. Seo, A.M. McDonagh, H.K. Shon, L. Tijing, Semiconductor photothermal materials enabling efficient solar steam generation toward desalination and wastewater treatment, Desalination 500 (2021) 114853.
[14] C.H. Huang, J.X. Huang, Y.H. Chiao, C.M. Chang, W.S. Hung, S.J. Lue, C.F. Wang, C.C. Hu, K.R. Lee, H.H. Pan, Tailoring of a piezo-photo-thermal solar evaporator for simultaneous steam and power generation, Adv. Funct. Mater. 31 (2021) 2010422.
[15] Y. Bu, Y. Zhou, W. Lei, L. Ren, J. Xiao, H. Yang, W. Xu, J. Li, A bioinspired 3D solar evaporator with balanced water supply and evaporation for highly efficient photothermal steam generation, J. Mater. Chem. A 10 (2022) 2856–2866.
[16] R. Djellabi, L. Noureen, V.-D. Dao, D. Meroni, E. Falletta, D.D. Dionysiou, C. L. Bianchi, Recent advances and challenges of emerging solar-driven steam and the contribution of photocatalytic effect, Chem. Eng. J. 431 (2022) 134024.
[17] S. Cao, A. Thomas, C. Li, Emerging materials for interfacial solar-driven water purification, Angew. Chem. 135 (2023) e202214391.
[18] M. Toyoda, M. Inagaki, Carbon materials for solar steam-generation, Carbon (2023) 118373.
[19] F. Wang, Y. Su, Y. Li, D. Wei, H. Sun, Z. Zhu, W. Liang, A. Li, Salt-resistant photothermal materials based on monolithic porous ionic polymers for efficient solar steam generation, ACS Appl. Energy Mater. 3 (2020) 8746–8754.
[20] K.W. Tan, C.M. Yap, Z. Zheng, C.Y. Haw, P.S. Khiew, W.S. Chiu, State-of-the-art advances, development, and challenges of metal oxide semiconductor nanomaterials for photothermal solar steam generation, Adv. Sustain. Syst. 6 (2022) 2100416.
[21] C. Sheng, N. Yang, Y. Yan, X. Shen, C. Jin, Z. Wang, Q. Sun, Bamboo decorated with plasmonic nanoparticles for efficient solar steam generation, Appl. Therm. Eng. 167 (2020) 114712.
[22] J. Liu, Q. Liu, D. Ma, Y. Yuan, J. Yao, W. Zhang, H. Su, Y. Su, J. Gu, D. Zhang, Simultaneously achieving thermal insulation and rapid water transport in sugarcane stems for efficient solar steam generation, J. Mater. Chem. A 7 (2019) 9034–9039.
[23] Y. Lin, H. Xu, X. Shan, Y. Di, A. Zhao, Y. Hu, Z. Gan, Solar steam generation based on the photothermal effect: from designs to applications, and beyond, J. Mater. Chem. A 7 (2019) 19203–19227.
[24] M.M. Mekonnen, A.Y. Hoekstra, Four billion people facing severe water scarcity, Sci. Adv. 2 (2016) e1500323.
[25] G. Liu, T. Chen, J. Xu, G. Yao, J. Xie, Y. Cheng, Z. Miao, K. Wang, Salt-rejecting solar interfacial evaporation, Cell Rep. Phys. Sci. 2 (2021).
[26] L. Zhang, X. Li, Y. Zhong, A. Leroy, Z. Xu, L. Zhao, E.N. Wang, Highly efficient and salt rejecting solar evaporation via a wick-free confined water layer, Nat. Commun. 13 (2022) 849.
[27] J. Yan, W. Xiao, L. Chen, Z. Wu, J. Gao, H. Xue, Superhydrophilic carbon nanofiber membrane with a hierarchically macro/meso porous structure for high performance solar steam generators, Desalination 516 (2021) 115224.
[28] P.-F. Liu, L. Miao, Z. Deng, J. Zhou, H. Su, L. Sun, S. Tanemura, W. Cao, F. Jiang, L.-D. Zhao, A mimetic transpiration system for record high conversion efficiency in solar steam generator under one-sun, Mater. Today Energy 8 (2018) 166–173.
[29] Y. Xia, Q. Hou, H. Jubaer, Y. Li, Y. Kang, S. Yuan, H. Liu, M.W. Woo, L. Zhang, L. Gao, Spatially isolating salt crystallisation from water evaporation for continuous solar steam generation and salt harvesting, Energy Environ. Sci. 12 (2019) 1840–1847.
[30] Q. Wang, F. Jia, A. Huang, Y. Qin, S. Song, Y. Li, M.A.C. Arroyo, MoS2@ sponge with double layer structure for high-efficiency solar desalination, Desalination 481 (2020) 114359.
[31] Y. Xiao, X. Wang, C. Li, H. Peng, T. Zhang, M. Ye, A salt-rejecting solar evaporator for continuous steam generation, J. Environ. Chem. Eng. 9 (2021) 105010.
[32] D. Zhao, X. Liu, Z. Shen, Effect of oxygen-containing functional groups on the wettability of coal through DFT and MD simulation, Arab. J. Chem. 16 (2023) 104606.
[33] D. Landolt, S. Mischler, Tribocorrosion of passive metals and coatings, Elsevier, 2011.
[34] J. Li, D. Song, K. Du, Z. Wang, C. Zhao, Performance of graphite felt as a cathode and anode in the electro-fenton process, RSC Adv. 9 (2019) 38345–38354.

[35] J. Gong, J. Li, J. Xu, Z. Xiang, L. Mo, Research on cellulose nanocrystals produced from cellulose sources with various polymorphs, RSC Adv. 7 (2017) 33486–33493.
[36] D. Galpaya, M. Wang, G. George, N. Motta, E. Waclawik, C. Yan, Preparation of graphene oxide/epoxy nanocomposites with significantly improved mechanical properties, J. Appl. Phys. 116 (2014).
[37] R. Djellabi, B. Yang, Y. Wang, X. Cui, X. Zhao, Carbonaceous biomass-titania composites with TiOC bonding bridge for efficient photocatalytic reduction of Cr (VI) under narrow visible light, Chem. Eng. J. 366 (2019) 172–180.
[38] R. Djellabi, B. Yang, K. Xiao, Y. Gong, D. Cao, H.M.A. Sharif, X. Zhao, C. Zhu, J. Zhang, Unravelling the mechanistic role of TiOC bonding bridge at titania/lignocellulosic biomass interface for Cr (VI) photoreduction under visible light, J. Colloid Interface Sci. 553 (2019) 409–417.
[39] A. Etale, A.J. Onyianta, S.R. Turner, S.J. Eichhorn, Cellulose: a review of water interactions, applications in composites, and water treatment, Chem. Rev. 123 (2023) 2016–2048.
[40] Z. Wu, H. Sun, Z. Xu, H. Chi, X. Li, S. Wang, T. Zhang, Y. Zhao, Underwater mechanically tough, elastic, superhydrophilic cellulose nanofiber-based aerogels for water-in-oil emulsion separation and solar steam generation, ACS Appl. Nano Mater. 4 (2021) 8979–8989.
[41] K. Nabeela, M.N. Thorat, S.N. Backer, A.M. Ramachandran, R.T. Thomas, G. Preethikumar, A.P. Mohamed, A. Asok, S.G. Dastager, S. Pillai, Hydrophilic 3D interconnected network of bacterial Nanocellulose/black titania photothermal foams as an efficient interfacial solar evaporator, ACS Appl. Bio Mater. 4 (2021) 4373–4383.
[42] P.L. Hurtado, A. Rouilly, V. Vandenbossche, C. Raynaud, A review on the properties of cellulose fibre insulation, Build. Environ. 96 (2016) 170–177.
[43] R. Pal, P. Goyal, S. Sehgal, Effect of cellulose fibre based insulation on thermal performance of buildings, Mater. Today.: Proc. 45 (2021) 5778–5781.
[44] J. Ali, L. Wang, H. Waseem, H.M.A. Sharif, R. Djellabi, C. Zhang, G. Pan, Bioelectrochemical recovery of silver from wastewater with sustainable power generation and its reuse for biofouling mitigation, J. Clean. Prod. 235 (2019) 1425–1437.
[45] L.F. Castañeda, F.C. Walsh, J.L. Nava, C.P. de Leon, Graphite felt as a versatile electrode material: properties, reaction environment, performance and applications, Electrochim. Acta 258 (2017) 1115–1139.
[46] Q. Yang, C. Xu, F. Wang, Z. Ling, Z. Zhang, X. Fang, A high-efficiency and low-cost interfacial evaporation system based on graphene-loaded pyramid polyurethane sponge for wastewater and seawater treatments, ACS Appl. Energy Mater. 2 (2019) 7223–7232.
[47] P. Wang, Emerging investigator series: the rise of nano-enabled photothermal materials for water evaporation and clean water production by sunlight, Environ. Sci.: Nano 5 (2018) 1078–1089.
[48] Y. Duan, C.D. Stinespring, B. Chorpening, Electronic structures, bonding configurations, and band-gap-opening properties of graphene binding with low-concentration fluorine, ChemistryOpen 4 (2015) 642–650.
[49] Z. Li, W. Cai, L. Song, Z. Gui, Y. Hu, X. Wang, A novel strategy to extend near-infrared light harvest of graphene for solar vapor generation and high-efficiency oil-water separation, Appl. Surf. Sci. 609 (2023) 155286.
[50] J. He, W. Han, H. Jiang, T. Zhang, X. Wang, B. Wang, C. Liu, C. Shen, Enhancing thermal localization efficiency in a wood-based solar steam generator with inverted-pyramid structure, Desalination 574 (2024) 117271.
[51] L. Zhu, M. Gao, C.K.N. Peh, G.W. Ho, Recent progress in solar-driven interfacial water evaporation: advanced designs and applications, Nano Energy 57 (2019) 507–518.
[52] Q. Jiang, L. Tian, K.K. Liu, S. Tadepalli, R. Raliya, P. Biswas, R.R. Naik, S. Singamaneni, Bilayered biofoam for highly efficient solar steam generation, Adv. Mater. 28 (2016) 9400–9407.
[53] K.-K. Liu, Q. Jiang, S. Tadepalli, R. Raliya, P. Biswas, R.R. Naik, S. Singamaneni, Wood–graphene oxide composite for highly efficient solar steam generation and desalination, ACS Appl. Mater. Interfaces 9 (2017) 7675–7681.
[54] L. Zhang, B. Tang, J. Wu, R. Li, P. Wang, Hydrophobic light-to-heat conversion membranes with self-healing ability for interfacial solar heating, Adv. Mater. 27 (2015) 4889–4894.
[55] G. Ni, S.H. Zandavi, S.M. Javid, S.V. Boriskina, T.A. Cooper, G. Chen, A salt-rejecting floating solar still for low-cost desalination, Energy Environ. Sci. 11 (2018) 1510–1519.
[56] J. Jiang, R. Yang, F. Zeng, S. Tu, Biomass-derived three-dimensional robust solar evaporator for efficient steam generation, water purification and salt-resistant desalination, Chem. Eng. J. 481 (2024) 148289.
[57] K. Yang, T. Pan, S. Dang, Q. Gan, Y. Han, Three-dimensional open architecture enabling salt-rejection solar evaporators with boosted water production efficiency, Nat. Commun. 13 (2022) 6653.
[58] S.K. Hazra, A.M. Saleque, A.K. Thakur, M.N.A.S. Ivan, D. Biswas, S.A. Khan, R. Saidur, Z. Ma, R. Sathyamurthy, Recent advancement in solar-driven interfacial steam generation for desalination: a state-of-the-art review, Energy Technol. 12 (2024) 2301190.